Applied Catalysis B: Environmental 166–167 (2015) 335–344

Contents lists available at ScienceDirect

Applied Catalysis B: Environmental

journal homepage: www.elsevier.com/locate/apcatb

Steam reforming of simulated biogas over plate Ni—Cr catalysts: Influence of pre-oxidation on catalytic activity

Quynh Thi Phuong Bui[a,c], Yongmin Kim[a], Sung Pil Yoon[a], Jonghee Han[a,b], Hyung Chul Ham[a,c], Suk Woo Nam[a,b,*], Chang Won Yoon[a,c,*]

[a] Fuel Cell Research Center, Korea Institute of Science and Technology, Hwarangno 14-gil 5, Seongbuk-gu, Seoul 136-791, Republic of Korea
[b] Green School, Korea University, 145 Anam-ro, Seongbuk-gu, Seoul 136-701, Republic of Korea
[c] Department of Clean Energy and Chemical Engineering, Korea University of Science and Technology, Daejeon, Republic of Korea

ARTICLE INFO

Article history:
Received 11 September 2014
Received in revised form
21 November 2014
Accepted 23 November 2014
Available online 29 November 2014

Keywords:
Steam reforming
Biogas
Ni—Cr
Plate catalyst
Pretreatment

ABSTRACT

The activity and stability of Ni—Cr plate catalysts were significantly enhanced by a pretreatment process involving pre-oxidation at ≥600 °C with subsequent reduction at 700 °C. Analytical techniques including SEM, TEM, and XPS-depth profiling studies revealed that the pretreatment induced surface reconstruction in the bulk Ni—Cr material generating new Ni sites with improved activity. The catalytic activity was highly dependent upon the oxidation temperature. In addition to the creation of novel Ni sites, chromium oxide acted as a structural promoter to suppress sintering of the Ni active sites. Activation of the Ni—Cr plate catalyst via pretreatment at 700 °C resulted in improved stability for biogas reforming reactions over a period of 100 h. Moreover, the stability of the reforming catalyst was sustained over 100 h with a steam/CH_4 ratio of ≥ 1.5. The influences of temperature, inlet H_2O/CH_4 ratio, and CH_4/CO_2 ratios on the steam reforming of biogas were further studied.

1. Introduction

To address current energy and environmental concerns, the biogas reforming for either hydrogen or syngas production has received considerable attention in recent years [1–5]. Biogas reforming with added steam provides an opportunity to employ carbon dioxide, one of the main constituents of biogas, as a C1 building block for fuel production [6]. Synthetic gas for high temperature fuel cells (HTFCs) including molten carbonate fuel cells (MCFCs) and solid oxide fuel cells (SOFCs) can be produced directly from biogas using Ni-based catalysts. These catalysts are widely employed for reforming reactions using H_2O and/or CO_2 as oxidants [7,8]. However, utilization of high operating currents in HTFCs results in increased cell temperatures and temperature gradients, which can decompose Ni catalysts in a stack [9,10]. Internal reforming of methane over a Ni-based catalyst is one strategy to recycle waste-heat potentially produced from a stack. For example, a Ni catalyst was efficiently used for the combined indirect and direct internal methane reforming to remove excess heat from an MCFC stack [11]. However, the physical instability of pure Ni powders results in rapid deactivation under HTFC operating conditions. Therefore, enhancing the thermal stability of stack components (e.g., catalysts) is necessary to improve the activity and durability of HTFCs under various operating conditions.

One strategy to increase the thermal and structural stability of bulk Ni catalysts for hydrogen production and HTFCs is the incorporation of Cr into the Ni material with structuralization to improve heat dissipation. For example, a disk-type porous Ni-10% Cr alloy catalyst, for the autothermal reforming of methane, has shown relatively high activity for H_2 generation and long-term stability [12]. For practical applications, however, the activity of a Ni alloy catalyst for methane reforming reaction requires improvement. Catalyst activity can be enhanced by either modification with additives or pretreatment. In the first instance, Sabirova et al. [13] reported 25% CH_4 conversion over a porous metallic Ni plate during steam reforming at 750 °C (H_2O/CH_4 = 2). Introduction of MgO into the Ni plate by the impregnation method helped increase the catalyst activity to 50–65%. In the case of pretreatment, a similar type of porous Ni catalyst had significantly increased activity for CO oxidation after an oxidation-pretreatment [14]. Moreover, Yan Ma et al. [15] used a sequential acid and alkali leaching process to enhance the catalytic activity of atomized Ni_3Al alloy. King et al. [16] claimed that a Ni–YSZ cermet in a SOFC produced NiO species dissolved in YSZ formed a solid solution during steam reforming and generated

* Corresponding authors at: Fuel Cell Research Center, Korea Institute of Science and Technology, Hwarangno 14-gil 5, Seongbuk-gu, Seoul 136-791, Republic of Korea. Tel.: +82 2 958 5262; fax: +82 2 958 5199.
E-mail addresses: cw.yoon@ust.ac.kr, cwyoon@kist.re.kr, swn@kist.re.kr (C.W. Yoon).

http://dx.doi.org/10.1016/j.apcatb.2014.11.045
0926-3373/

small Ni particles following hydrogen pretreatment. However, the active sites produced by pretreatment in this case were unstable under the reaction conditions and subsequently deactivated. In a more recent study, Bonura and coworkers developed a highly active NiCu alloyed catalyst supported on $Ce_{0.9}Gd_{0.1}O_{2-\delta}$ (NiCu/CGO) for integrated biogas SOFC process and proved that NiCu/CGO suppressed coke deposition as well as metal sintering upon its utilization as a SOFC anodic material, thereby effectively stabilizing the active metal sites for biogas dry reforming [17].

In this study, we elucidated the influence of the pretreatment process, pre-oxidation at ≥600 °C with sequential reduction at high temperature (700 °C), on the catalytic activity of a Ni—Cr plate catalyst for the steam reforming of biogas. Pretreated catalysts showed increased activity over the as-prepared Ni—Cr catalysts for reforming reactions conducted at 700 °C. In addition, the Ni—Cr plate catalyst activated by pretreatment exhibited superior stability over a time period of 100 h. Controlling factors including temperature, inlet H_2O/CH_4 ratio, and CH_4/CO_2 ratios for the steam reforming of biogas were also identified.

2. Experimental

2.1. Preparation of the porous plate-type Ni—Cr catalyst

Isopropyl alcohol, binder (Methyl Cellulose #1500, Junsei Chemical. Co., Japan), plasticizer (Glycerol, Junsei Chemical Co., Japan), defoamer (SN-154, San Nopco Korea), deflocculant (Cerasperse-5468, San Nopco Korea), dispersant (polyacrylic acid), Ni metal (INCO. #255, INCO), and Cr metal (Alfa > 99.9%) were purchased as received. A mixture containing the Ni and Cr powders (or only Ni powder), plasticizer, defoamer, deflocculant, dispersant, and distilled water was initially ball-milled for 15 h. Following the addition of polyethylene oxide, the second ball milling was carried out for 6 h. Next, small amounts of methyl-cellulose and isopropyl alcohol as a de-airing agent were added to the resulting ball-milled slurry. The third ball milling was then performed for 1 h, followed by air removal under vacuum. Green sheet is made by use of a doctor blade in which tape casting was done with de-airing slurry and drying sufficiently at ambient temperature. Afterwards, Ni—Cr or Ni green sheet was sintered at 1000 °C in H_2/Ar atmosphere to achieve Ni—Cr alloy plate or Ni plate. The porous Ni and Ni—Cr plate after the sintering process had the thickness of 0.85 mm and 1.0 mm with porosity of 75% and 59% (ASTM), respectively. The resulting plates were cut into circular shapes with inner and outer diameters of 8.0 mm and 50 mm, respectively, for catalytic tests [12]. The resulting Ni—Cr catalyst possesses 90 wt% Ni and 10 wt% Cr.

2.2. Catalytic reforming of biogas over porous Ni—Cr plate catalysts

Catalytic reactions were carried out in a reactor with a cylindrical stainless steel housing and plate-type catalyst layers. The Ni—Cr plate catalyst was cut into circular shaped pieces with outer and inner diameters of 50 mm and 8 mm, respectively. The weight of the plate was 5.6 g. The catalyst was then sandwiched between two Inconel sheets that served as flow paths. The layers were fixed in the reactor by a two disk-type end plate made of stainless steel [12]. The reactor was placed in a furnace and heated to the desired operating temperature (500–700 °C) under N_2 with a heating rate of 5 °C/min, following pretreatment and reforming reactions. A *K*-type thermocouple was placed in a hole located in the upper end plate gas outlet to monitor the reaction temperature. If necessary, the Ni—Cr plate catalysts were pretreated under the following conditions: Pre-oxidation of the catalytic materials at the desired temperature range from 500 °C to 700 °C for 2 h in air (1000 mL/min) followed by reduction using 20% H_2/N_2 (200 mL H_2/800 mL N_2) at 700 °C for 1 h. All reforming reactions were carried out at 700 °C at atmospheric pressure. A simulated biogas fuel containing CH_4 and CO_2 was introduced into the reactor with steam and N_2 in a total inlet flow rate of 1600 mL/min ($H_2O/CH_4/CO_2/N_2$

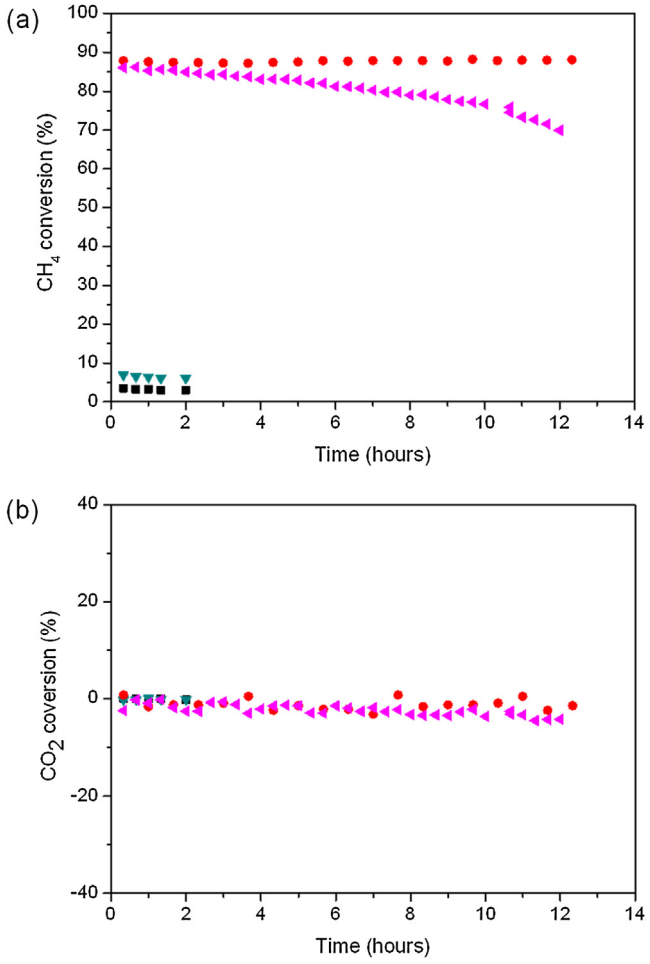

Fig. 1. Influence of pre-oxidation temperatures on (a) CH_4 conversion and (b) CO_2 conversion over Ni-Cr catalysts: (■) without pre-oxidation, (▼) 500 °C, (◄) 600 °C, (●) 700 °C.

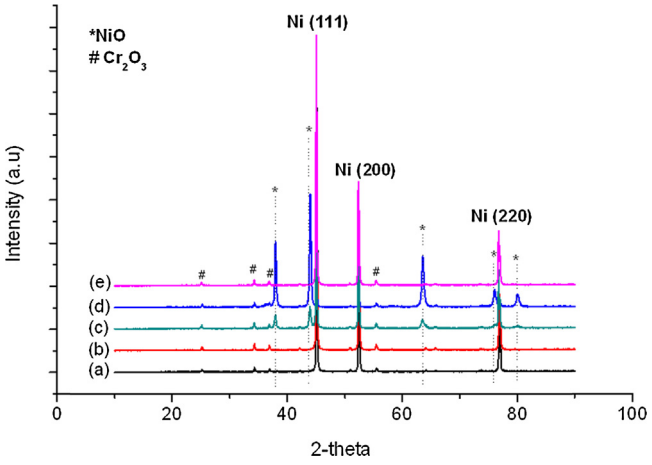

Fig. 2. XRD patterns of the Ni—Cr catalysts: (a) without oxidation, (b) after oxidation at 500 °C, (c) after oxidation at 600 °C, (d) after oxidation at 700 °C, (e) after oxidation at 700 °C, followed by reduction. (For interpretation of the references to color in the text citation of this figure, the reader is referred to the web version of this article.)

ratios of 2.0/1.0/0.57/1.7). Water was vaporized and mixed with the inlet gas before transporting to the reactor. The composition of the effluent gases, following removal of steam with a cold trap, were determined with a gas chromatograph (HP6890 Series II) equipped with dual TCD detectors using Ar and He as carrier gases. N_2 was used as the reference gas in the GC analyses to quantify the product gases and gas conversions. CH_4 and CO_2 conversions and the H_2 yield are determined as follows:

$$\%\,CH_4 \text{ conversion} = \frac{F_{CH_4 in} - F_{CH_4 out}}{F_{CH_4 in}} \times 100$$

$$\%\,CO_2 \text{ conversion} = \frac{F_{CO_2 in} - F_{CO_2 out}}{F_{CO_2 in}} \times 100$$

$$H_2 \text{ yield} = \frac{F_{H_2 product}}{F_{CH_4 in}}$$

where $F_{CH_4 in}$ and $F_{CO_2 in}$ denote the rates of inlet molar flow; $F_{CH_4 out}$, $F_{CO_2 out}$, and $F_{H_2 product}$ represent the rates of outlet molar flow.

2.3. Materials characterization

X-ray diffraction (XRD, RigakuMinilex II) analyses were performed using Cu K_α radiation (λ = 1.5406 Å) with 2-theta ranging from 0° to 90°. X-ray photoelectron spectroscopy (XPS) was performed with a PHI 5000 VersaProbe (Ulvac-PHI) system using monochromatized Al K_α (1486.6 eV) radiation under a background pressure of about 10^{-10} Torr with a spot size of 100 μm × 100 μm. The measured binding energies were calibrated by the C1s line (284.6 eV) from carbon contamination. For XPS depth-profiling studies, the samples were sputtered under Ar^+ ion beams (3 keV) rastering on the surface over an area of 2 mm × 2 mm.

Changes in surface morphology for the as-prepared and pretreated catalysts were monitored using scanning electron microscopy (FEG-ESEM, Philips FEI XL-30) and transmission electron microscopy/electron dispersive spectroscopy (TEM/EDS, FEI-Technai G2F20). The samples were treated using a FEI-Helios Focused-Ion Beam, followed by characterization with TEM. Thermal gravimetric analysis (TGA) was conducted in a quartz tube reactor. Changes in weight for the square-shaped samples with a fixed area of 1.79 cm^2 were observed isothermally.

Brunauer–Emmett–Teller (BET) surface areas were determined by N_2 adsorption at −196 °C using an ASAP 2010 Micrometrics instrument. The BET surface area of the bulk Ni—Cr material was measured to be 0.22 m^2/g.

Temperature programmed reduction (TPR) was carried out using a BELCAT – M apparatus. In a quartz micro-reactor, a desired sample was pretreated in Ar at 300 °C and then cooled down to room temperature. The mixture of 5% H_2/Ar was then supplied to the reactor with a flow rate of 30 mL/min. The reactor was programmatically heated to 950 °C using a heating rate of 10 °C/min. The H_2 consumption was monitored by a thermal conductivity detector (TCD).

3. Results and discussion

3.1. Influence of pretreatment on catalytic activity

Steam reforming reactions of simulated biogas were initially conducted over bulk Ni—Cr catalysts at 700 °C with the $H_2O/CH_4/CO_2/N_2$ ratios of 2/1/0.57/1.7. The ratio of H_2O/CH_4 = 2 was chosen to prevent significant carbon deposition during reforming. As depicted in Fig. 1a, the bulk Ni—Cr plate catalyst showed very low activity with an approximate CH_4 conversion of 5%. Next, a pretreatment process was employed to enhance the activity of the catalyst by partly oxidizing the as-prepared Ni—Cr material in situ under air for 2 h at different temperatures ranging from 500 to 700 °C, followed by reduction with 20% H_2/N_2 for 1 h at 700 °C. The CH_4 conversion of the catalyst pre-oxidized at 500 °C only increased to ca. 8%. In contrast, the activities of the pre-oxidized catalysts at ≥600 °C were significantly enhanced. The observed CH_4 conversion with the catalyst pre-oxidized at 600 °C was initially 85%, but then decreased to 70% after 12 h. In contrast, pre-oxidation of the Ni—Cr material at 700 °C afforded a CH_4 conversion of 86%, which was maintained over the 12 h test period. The CO_2 conversions for all experiments were found to be nearly zero (Fig. 1b), which indicated that the dominant process was steam reforming of methane instead of CO_2 reforming of methane.

3.2. Characterization of the pretreated Ni—Cr catalysts

To understand the enhanced catalytic activities produced by the pre-oxidation process, the Ni—Cr catalysts were characterized by XRD, SEM, TEM-EDS, and XPS before and after pretreatment. The XRD patterns of the bulk Ni—Cr catalyst primarily contained the Ni crystal planes (1 1 1), (2 0 0), and (2 2 0) with only trace amounts of Cr_2O_3 (Fig. 2). This implies that the chromium species were partly oxidized prior to their diffusion into the existing Ni lattice during the fabrication procedure [18]. Following the

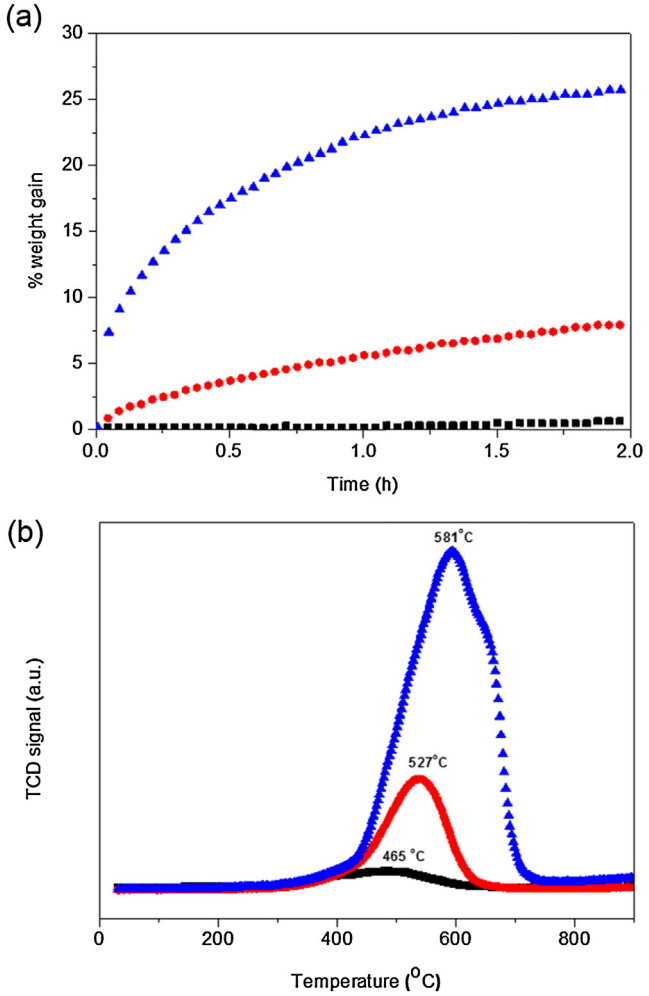

Fig. 3. (a) TGA profiles of the Ni—Cr catalysts in air at 500 °C (■, black), 600 °C (●, red), and 700 °C (▲, blue); (b) TPR profiles of the Ni—Cr catalysts pre-oxidized at 500 °C (■, black), 600 °C (●, red), and 700 °C (▲, blue). (For interpretation of the references to color in this figure legend, the reader is referred to the web version of this article.)

pre-oxidation of the Ni—Cr alloys at 500 °C, the main peaks for the Ni crystal planes still existed, and the formation of NiO species was negligible (Fig. 2, red). Increasing the pre-oxidation temperature to ≥600 °C significantly increased the quantities of NiO species (Fig. 2, green and blue). Reduction of the NiO species formed by oxidation at 700 °C resulted in increased intensities for Ni(0) species while intensities for the Cr_2O_3 species remained unchanged (Fig. 2e). The TGA experiments were consistent with the XRD results, which showed the weight of the catalyst increased more rapidly at higher oxidation temperatures. The weight increase mainly resulted from the formation of NiO: 700 °C (26 wt%) > 600 °C (8.1 wt%) > 500 °C (0.65 wt%) (Fig. 3a). According to the TPR analyses (Fig. 3b), the peaks correspond to the Ni—Cr catalysts oxidized at 500 °C, 600 °C and 700 °C were appeared at ca. 465 °C, 527 °C and

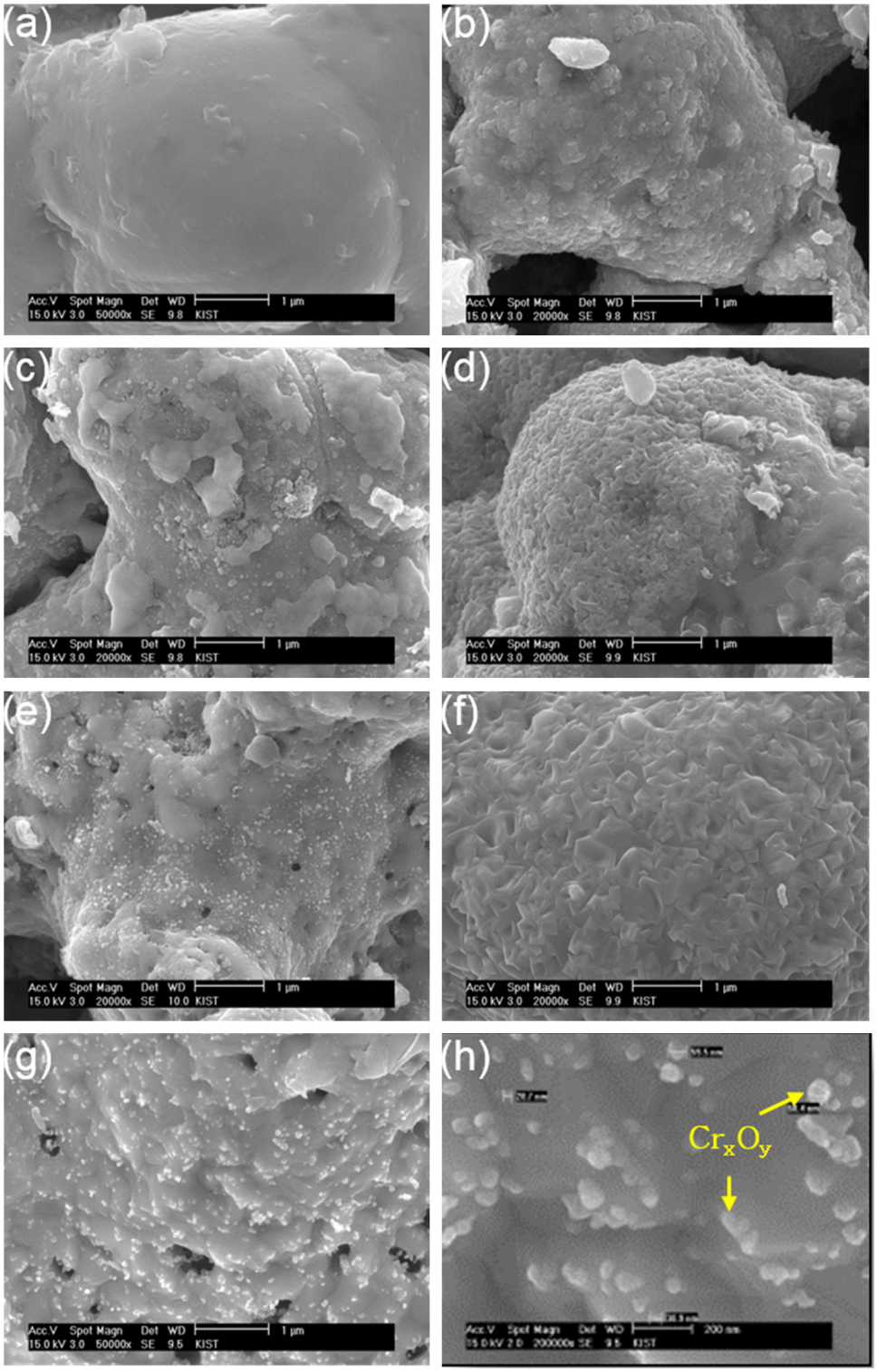

Fig. 4. SEM images of the Ni—Cr catalysts: (a) the surface of bulk Ni—Cr, (b) after oxidation at 500 °C, (c) after oxidation at 500 °C followed by reduction at 700 °C, (d) after oxidation at 600 °C, (e) after oxidation at 600 °C followed by reduction at 700 °C, (f) after oxidation at 700 °C, and (g) after oxidation at 700 °C followed by reduction at 700 °C, and (h) the enlarged figure of (g) with the scale bar of 200 nm. The scale bars of (a)–(g) are 1 μm.

581 °C, respectively. The increased reduction temperature along with the significantly increased peak area for the Ni—Cr catalyst oxidized at 700 °C indicates the formation of increased amounts of oxide species and further suggests enhanced interaction between NiO and Cr_2O_3. The surface areas of the catalysts after the pretreatment processes increased slightly: For Ni—Cr oxidized at 600 °C followed by reduction, 0.84 m^2/g; for Ni—Cr oxidized at 700 °C followed by reduction, 1.64 m^2/g. Since the Ni(0) species are likely the active sites for the desired biogas reformation, the extent of NiO formation may be associated with catalytic activity and stability following reduction (vide infra).

The surface morphology of the Ni—Cr catalyst was monitored by SEM before and after pretreatment (Fig. 4). As depicted in Fig. 4a, the original surface of the as-prepared Ni—Cr plate consists of Ni—Cr alloy particles where the Cr_2O_3 species are likely the relatively bright-colored agglomerates [19]. Upon oxidation at 500 °C and subsequent reduction at 700 °C, the Ni—Cr surface became wrinkled and oxide species further appeared (Fig. 4b). These oxide species appeared to develop in a uniform fashion and progressively covered the entire catalyst surface as the pre-oxidation temperature increased to 600 °C (Fig. 4d). Pre-oxidation of the catalyst at 700 °C led to a significant volumetric expansion along with anisotropic growth of the oxide species (Fig. 4f). Moreover, reduction of the oxidized Ni—Cr material changed its surface structure remarkably (Fig. 4c, e, and g). These results suggest that introduction and subsequent removal of oxygen from the as-prepared Ni—Cr catalyst at high temperatures (600 °C and 700 °C) generated a number of bright-colored fine particles with small pores that were uniformly dispersed over the surface. An enlarged SEM image (Fig. 4h) shows the surface reconstruction induced by the pretreatment process (oxidation and sequential reduction). The newly formed fine bright-colored particles with an average size ranging from 20 to 70 nm protrude from the rough surface. Fig. 5 shows the cross-sectional TEM image of an intraparticle pore composed of bulk Ni substrate (yellow circle), Ni-rich particle supported Cr_xO_y (blue circle), and pure Cr_xO_y grains (red circle).

Catalyst compositions were further analyzed by XPS-depth profiling studies where Ar^+ ions were sputtered into the material using a sputtering rate of 40 nm min^{-1} followed by in situ analyses using XPS. Since surface reconstruction for the pre-oxidation process at 500 °C was insignificant (Fig. 4c and d), only the catalysts pre-oxidized at 600 °C and 700 °C were employed for this study. For comparison, the pre-oxidized Ni—Cr surface was further reduced and analyzed under the same conditions. Analysis of the as-prepared Ni—Cr catalyst showed uniform distribution of Ni, Cr, and O (Fig. 6a). The oxidized Ni—Cr catalysts had relatively high oxygen content throughout the material (Fig. 6b). Catalysts oxidized at 600 °C and 700 °C exhibited predominant peaks at ca. 854 eV with a broad shoulder centered at ca. 856 eV (Fig. 6c). These results indicate the presence of a NiO phase [19,20] as well as other Ni containing species including $NiCr_2O_4$ [21], NiOH, and/or defect Ni^{3+} [19,20,22]. For the catalyst pre-oxidized at 600 °C, peaks corresponding to metallic Ni(0) species centered at ca. 852 eV [19,20] increased gradually and became the predominant phase in the inner region of the material (Fig. 6c). Furthermore, the catalyst oxidized at 600 °C had a higher Ni(0) intensity than that oxidized at 700 °C in the inner region (about 150 nm depth from the surface). This indicates that oxidation was limited at 600 °C, but occurred uniformly throughout the material at 700 °C. Oxidation at 700 °C also afforded a higher concentration of chromium oxide than the oxidation at 600 °C within the depth range of ca. 100 nm. A binding energy for $Cr2p_{3/2}$ of ca. 576 eV (Fig. 6d) was attributed to the formation of Cr_2O_3 (Cr^{3+}) species [23]. The O1s spectrum showed a broad peak in the range of 529–531 eV with a maximum centered at ca. 529 eV (Fig. 6e), which likely results from oxygen present in nickel oxides, chromium oxides, adsorbed hydroxides,

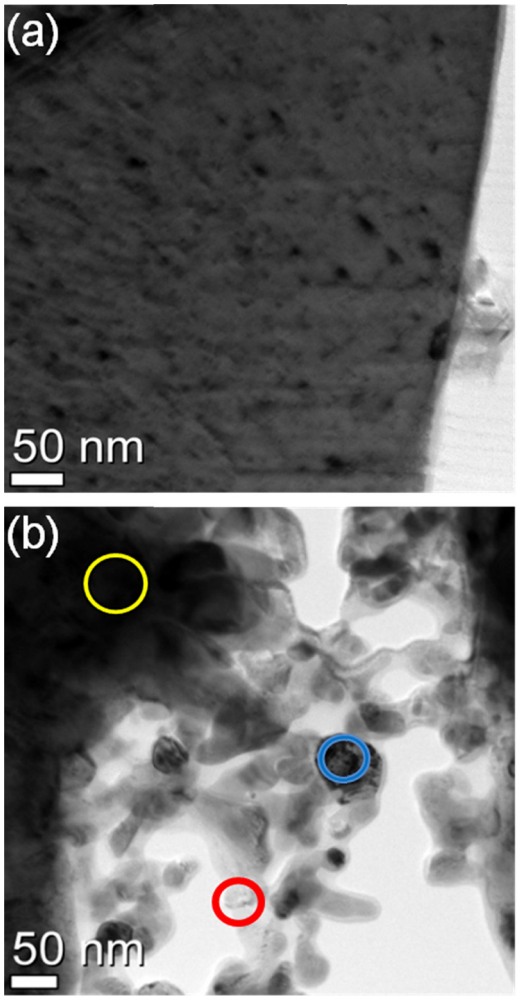

Fig. 5. The cross sectional TEM-EDS images of the Ni—Cr catalyst: (a) before pretreatment and (b) after pretreatment. Yellow, blue, and red circles represent Ni, $NiCrO_x$, and Cr_2O_3 enriched regions, respectively, evidence by EDX (see Fig. S1 in the supporting material). (For interpretation of the references to color in the text citation and legend of this figure, the reader is referred to the web version of this article.)

and adsorbed water [21,22]. Upon reduction of the oxidized catalysts, the Ni—Cr catalyst oxidized at 700 °C was found to have higher concentration of chromium oxides at its surface compared to that oxidized at 600 °C (Fig. 7a). In addition, nearly all nickel oxide species appeared to be reduced to Ni(0) with a binding energy of ca. 852 eV (Fig. 7b). In contrast, little change in the binding energies of the chromium species (ca. 576 ± 0.2 eV) were found, which indicated that Cr_2O_3 was not reduced under the conditions employed (Fig. 7c). Compared to those of the oxidized catalysts at 600 °C and at 700 °C (Fig. 6e), the O1s peaks of the reduced Ni—Cr catalysts were slightly shifted into higher energies with a maximum centered at ca. 530.5 eV (Fig. 7d), which could mainly be contributed by oxygen species from Cr_2O_3.

Based on XPS-depth profiling studies, the active sites generated in the pretreatment process shown in the SEM image (Fig. 4h) were attributed to Ni(0) supported on Cr_2O_3. While both Ni and Cr elements were initially oxidized by O_2, the NiO species formed were readily reduced while the Cr_2O_3 species were poorly reduced under the conditions employed. The remaining Cr_2O_3 species served as supports for the reduced Ni(0) species. The resulting Ni^0/Cr_2O_3 species were likely responsible for the enhanced catalytic activity and stability (vide infra).

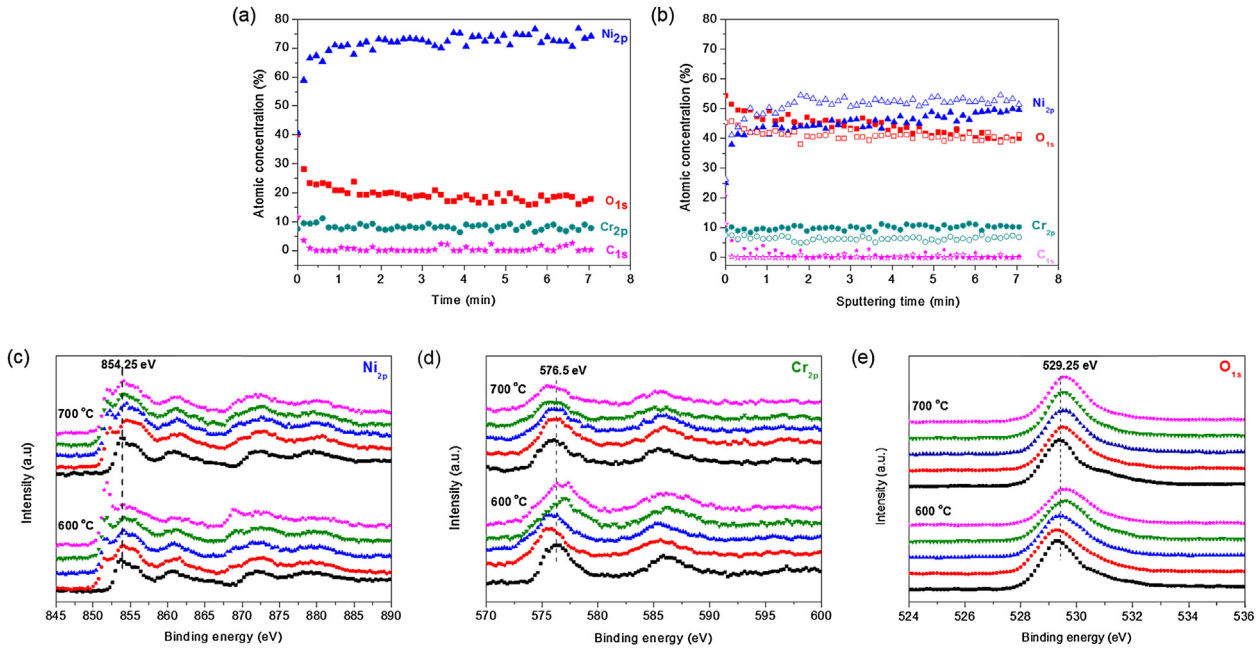

Fig. 6. XPS depth-profiling data for the Ni—Cr catalysts: (a) the prepared Ni—Cr plate; (b) after oxidation at 600 °C for 2 h (solid symbol) and at 700 °C for 2 h (open symbol); (c, d and e) the corresponding XPS spectra after sputtering for 0 min (■, black), 1.2 min (●, red), 2.4 min (▲, blue), 3.6 min (▼, green), and 7.2 min (★, pink). (For interpretation of the references to color in this figure legend, the reader is referred to the web version of this article.)

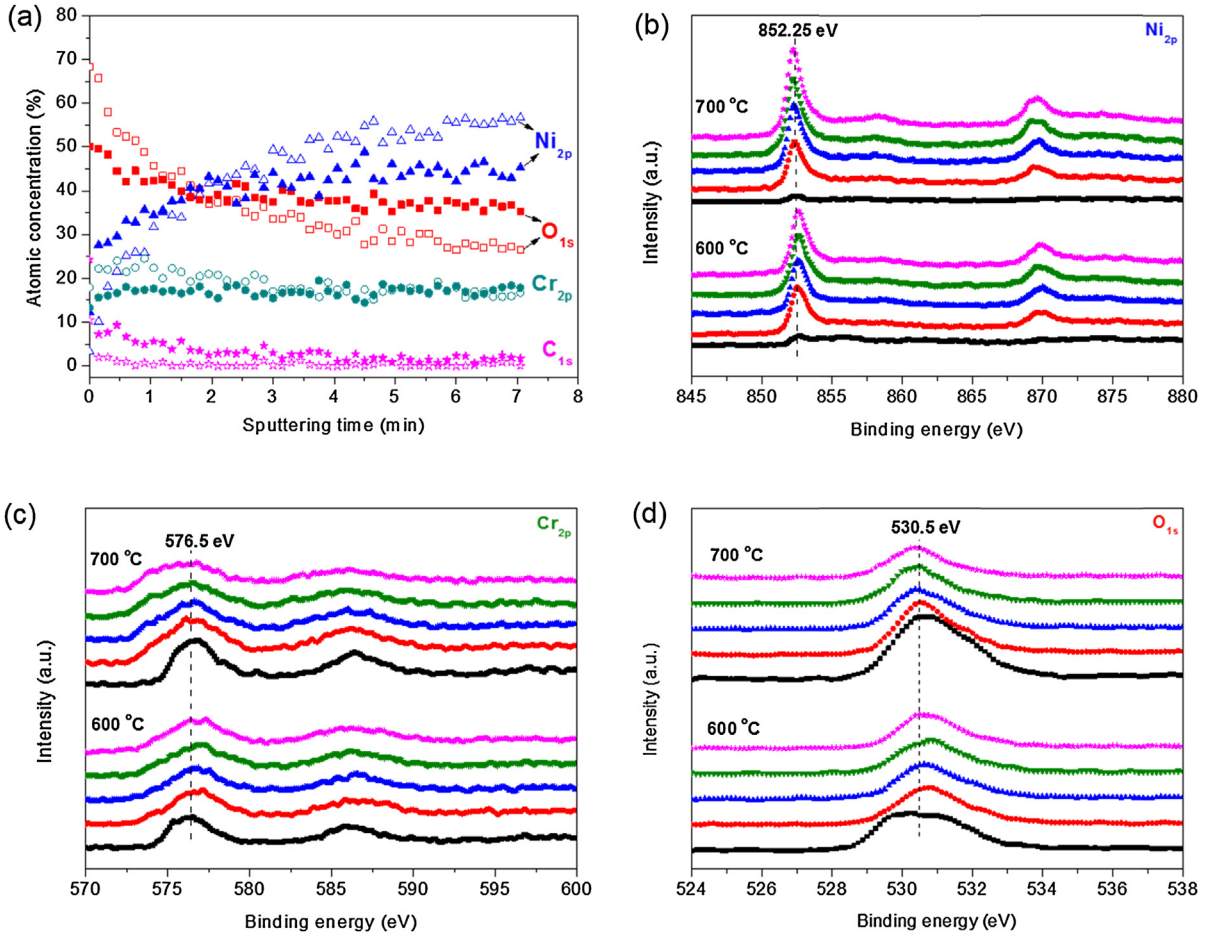

Fig. 7. XPS depth-profiling data of the pre-oxidized Ni—Cr catalysts after reduction in H_2/N_2 at 700 °C for 1 h: (a) pre-oxidation at 600 °C (solid symbol) and at 700 °C (open symbol); (b–d) the corresponding XPS spectra of the pretreated Ni—Cr catalysts after sputtering for 0 min (■, black), 1.2 min (●, red), 2.4 min (▲, blue), 3.6 min (▼, green), and 7.2 min (★, pink). (For interpretation of the references to color in this figure legend, the reader is referred to the web version of this article.)

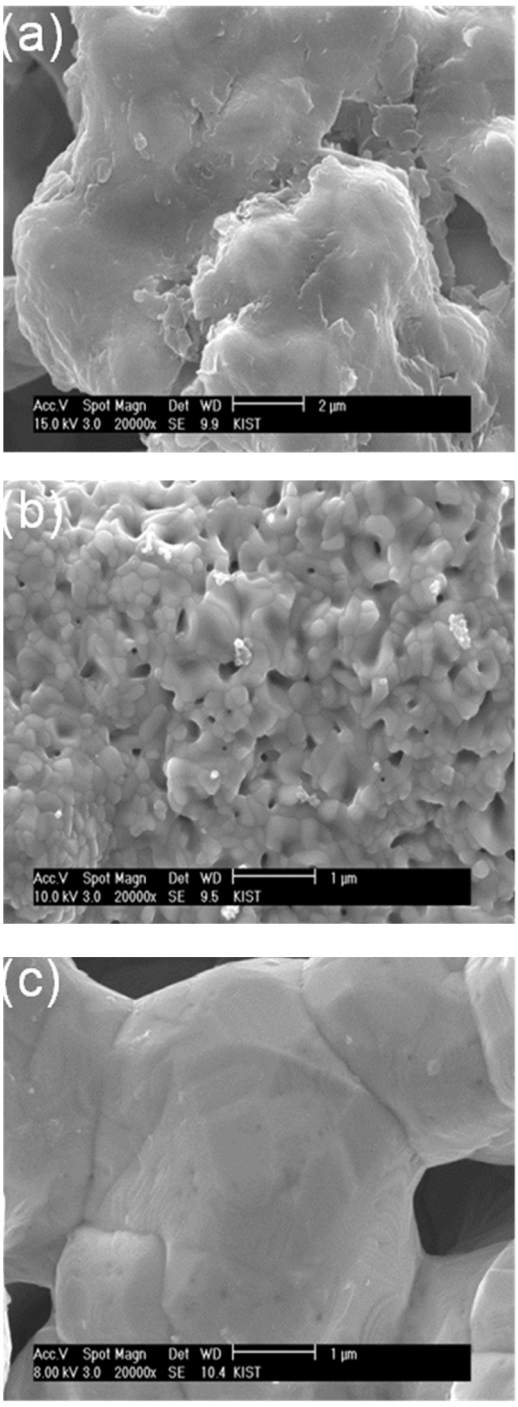

Fig. 8. SEM images of the metallic Ni catalyst: (a) bulk Ni plate, (b) after oxidation at 700 °C, and (c) after oxidation at 700 °C followed by reduction in H_2/N_2 at 700 °C.

3.3. Mechanistic consideration for the reconstruction of Ni active sites in the Ni—Cr catalyst

The pretreatment process for the Ni—Cr catalyst is crucial for activating and stabilizing the active sites for CH_4 reforming because the Ni—Cr materials pre-oxidized at ≥600 °C showed significantly improved activity and stability (Fig. 1). Furthermore, various characterization methods indicated that pre-oxidation produced changes in the morphology of the catalyst, which were influenced by oxidation temperature. The reported mechanism for oxidation of Ni—Cr alloys is dependent upon alloy composition, surface perfection, oxidation temperature, and oxidation time

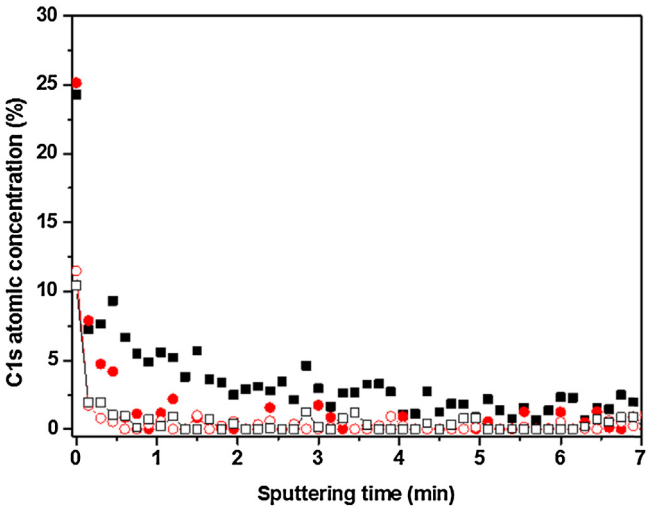

Fig. 9. C1s depth-profiles of the pretreated Ni—Cr catalysts: after reduction following oxidation at 600 °C (■, black) and after reforming for 12 h (□); after reduction following oxidation at 700 °C (●, red) and after reforming for 12 h (○). (For interpretation of the references to color in this figure legend, the reader is referred to the web version of this article.)

[24–26]. The extraction of fine Ni nanoparticles from bulk Ni-based catalysts was reported to enhance catalytic activity in methane steam reforming [15,16]. In addition, internal and external oxidation processes were proposed to occur during the oxidation process [25,26]. Mechanical stresses caused by oxide growth likely induced the formation of cracks and pores inside the particles upon continued oxidation. These cracks and pores could then promote oxygen mobility to drive internal oxidation for both nickel and chromium. Coalescence of such vacancies may lead to the formation of intraparticle pores [26,27]. Several theoretical and experimental investigations suggested that low-coordinated atoms located at steps and/or other defect sites were more reactive than those at close-packed surfaces, and smaller particles were likely to possess more active sites [28,29]. Similarly, defect sites are believed to be reactive in the initiation of water dissociation [30,31]. Reactivity toward methane adsorption and dissociation was also found to be dependent upon the structure of the active sites [32,33].

Based on the combined results of this study and others, a plausible pathway for the creation of new active sites by surface reconstruction in the Ni—Cr catalyst is proposed. This mechanism involves: (i) formation of a NiO phase in the Ni—Cr plate during the pre-oxidation process, (ii) production of oxygen vacancies and Ni(0) species in the NiO lattice by reduction, (iii) formation of anisotropic grains, grain boundaries, intraparticle pores, etc. in the new surface by rearrangement of the vacancies, and (iv) generation of Ni(0) nanoparticles supported by unreduced Cr_2O_3 during the surface reconstruction. This mechanism is consistent with the observation of intraparticle pores and fine particles dispersed on a rough substrate enriched with defects. In addition, the chromium-depleted regions in the SEM images (Fig. 5) likely originated from the partially sintered Ni(0) species following the reduction of the nickel oxides. The significantly improved activity produced by the pretreatment process for the Ni—Cr catalyst likely resulted from creation of new active sites, Ni(0) and/or Ni(0)/Cr_2O_3, located at pores, steps, and other defect sites. The reduced activity for the as-prepared Ni—Cr material may be due to its close-packed structure, which is unlikely to promote dissociation of CH_4 because of the high activation energy for CH_4 cracking [28].

Chromium oxide species (Cr_2O_3) have a potentially important role in preventing the sintering of reduced nickel species upon the removal of oxygen. For example, chromium oxides are considered as structural promoters for stabilizing the newly generated active

sites. To elucidate the role of Cr_2O_3 in stabilizing the reconstructed Ni active sites, further studies were conducted with a metallic bulk nickel plate. The bulk nickel plate was pre-oxidized at 700 °C, followed by reduction at the same temperature. In the absence of Cr_2O_3, the bulk nickel species appeared to be sintered back to a closed-packed structure after reduction (Fig. 8). The CH_4 conversion of this pretreated Ni plate was <20%. This result strongly supports the critical role of chromium oxide in stabilizing the newly generated Ni active sites, thereby promoting the CH_4 reforming reactions. The role of supporting oxides in suppressing catalyst deactivation caused by sintering was also observed in the previous study where nickel species were stabilized in perovskite oxides for ethanol reforming reactions [34].

To understand the observed deactivation for the catalyst pre-oxidized at 600 °C during the reforming reaction (Fig. 1), further XPS-depth profiling studies were conducted (Fig. 9). The C1s (binding energy at 285 eV) concentration for the catalyst pre-oxidized at 600 °C continuously decreased to zero after ca. 12 h on stream, indicating that the initially formed carbon species were gasified by steam during reforming. This result suggests that catalyst deactivation resulted from loss of active sites caused by sintering rather than carbon deposition under the conditions employed. Therefore, the low concentration of Cr_2O_3 created at 600 °C was insufficient to suppress sintering of the active sites since chromium oxide stabilized the Ni active sites.

3.4. Steam reforming of simulated biogas

The long-term stability of the Ni—Cr plate catalyst was initially explored by varying temperatures in the range of 600–700 °C. Prior to the biogas and steam supply, all catalysts were pre-oxidized in air at 700 °C for 2 h, followed by reduction in H_2/N_2 at 700 °C for 1 h. As depicted in Fig. 10a, CH_4 conversions increased as temperatures increased: 53% at 600 °C, 73% at 650 °C, and 87% at 700 °C. These activities were maintained until 100 h on stream with slight degradation of 2–4%. Likewise, CO_2 conversions were found to be higher with higher temperatures (Fig. 10b). For instance, the conversion at 600 °C was calculated at −40% while at 700 °C it was close to zero. The significantly decreased CO_2 conversion at 600 °C was likely caused by the water gas shift (WGS) reaction occurring at this temperature. The WGS reaction is less favorable at high temperature, thus increasing the reaction temperature to 700 °C increased the CO_2 conversion close to its equilibrium value of 1.7%. These results may imply that the rate of CO_2 production via WGS may be comparable to consumption by CO_2 reforming of CH_4 at 700 °C. The syngas ratios of H_2/CO decreased as temperature increased, whereas the H_2 yields increased as temperature increased (Fig. S2). The morphological studies indicated that the surface of the pretreated Ni—Cr catalyst appears to be partly agglomerated after

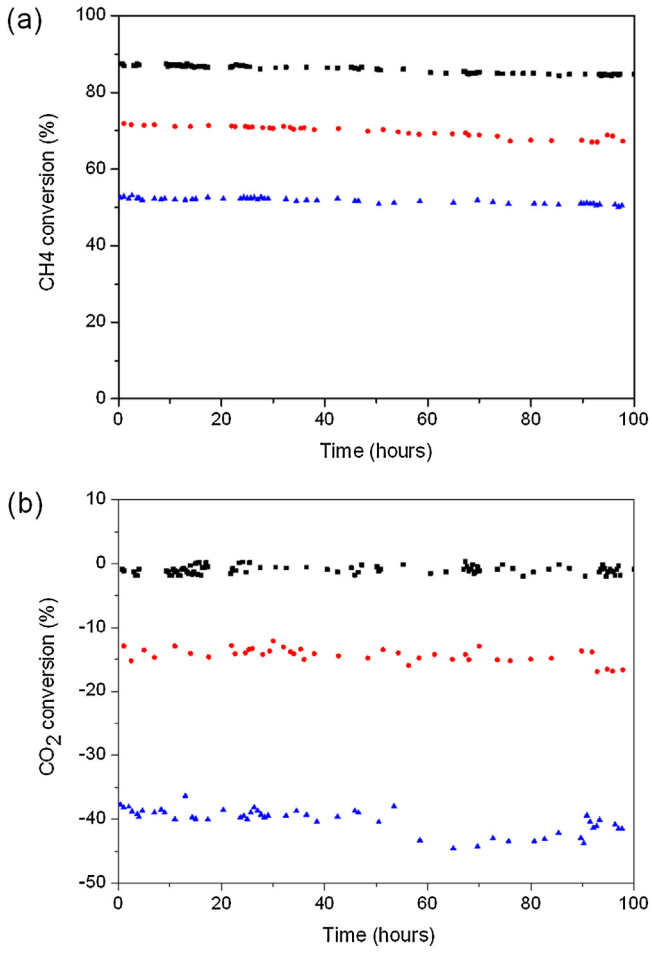

Fig. 10. Effect of temperature on the catalytic activity of the pretreated Ni—Cr catalysts (▲, 600 °C; ●, 650 °C; ■, 700 °C): (a) CH_4 conversion and (b) CO_2 conversion. Reforming reactions were performed using the following conditions: steam/CH_4/CO_2/N_2 = 2/1/0.57/1.7 and GHSV = 50,000 h^{-1}.

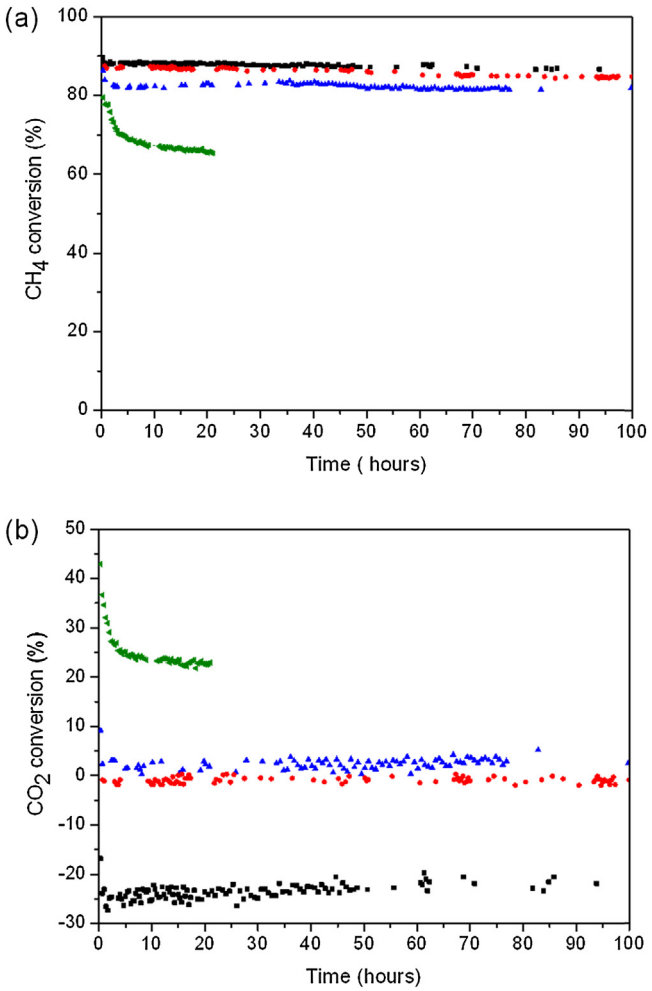

Fig. 11. Effect of the steam/CH_4 (S/C) ratios on catalytic activity of the pretreated Ni—Cr catalysts (◄, S/C = 1; ▲, S/C = 1.5; ●, S/C = 2; ■, S/C = 3): (a) CH_4 conversion and (b) CO_2 conversion. Reforming reactions were performed using the following conditions: a CH_4/CO_2 ratio of 1.76, a temperature of 700 °C, and a GHSV of 50,000 h^{-1}.

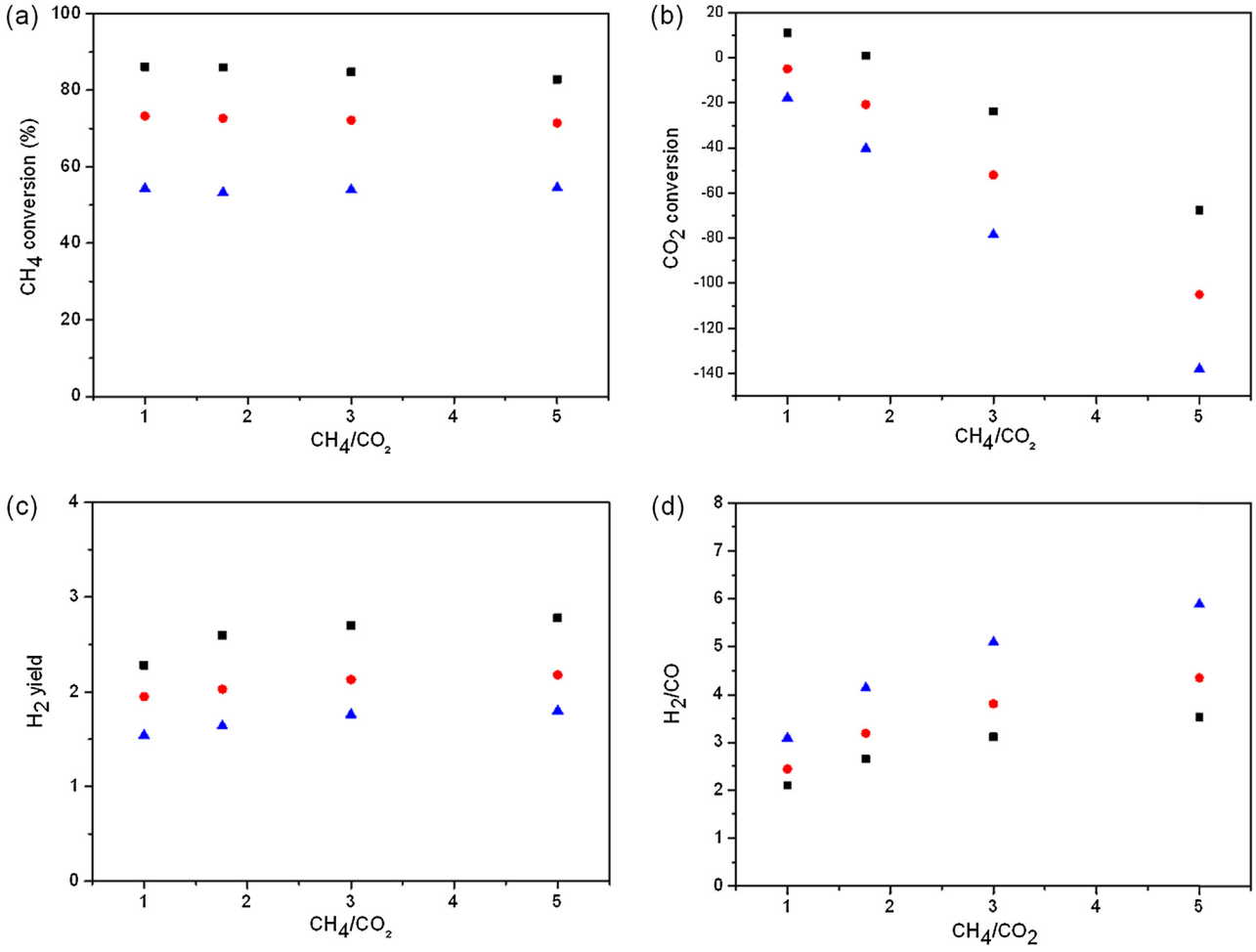

Fig. 12. Effect of inlet CH_4/CO_2 on catalytic activity of the pretreated Ni—Cr catalysts (▲, 600 °C; ●, 650 °C; ■, 700 °C): (a) CH_4 conversion, (b) CO_2 conversion, (c) H_2 yield and (d) H_2/CO ratio. Steam/CH_4 = 2 and GHSV = 50,000 h^{-1}.

100 h, but the catalyst still possessed open active sites readily accessible by reactants.

To determine the quantity of steam required to minimize the effect of carbon deposition on activity and stability of the pretreated Ni—Cr catalysts, the biogas reforming reactions utilizing CH_4, CO_2, and H_2O were monitored for 100 h with varying inlet H_2O/CH_4 (S/C) ratios. The pretreated Ni—Cr catalyst afforded CH_4 conversions of 87% and 88% with S/C ratios of 2 and 3, respectively (Fig. 11a). For an S/C of 1.5, the initial activity of 87% dropped to 82% within 1 h and was maintained at this level. However, an initial CH_4 conversion of 80% quickly decreased upon utilization of an S/C of 1, which was presumably due to the carbon deposition. Consistent with this result, an initial CO_2 conversion of 45% decreased significantly when an S/C ratio of 1 was employed (Fig. 11b). The CO_2 conversions obtained for S/C = 1.5 and 2 were close to 0%, whereas they decreased remarkably to −25% at S/C = 3. The H_2 yield and H_2/CO ratio increased with an increase in the S/C ratio (Fig. S3).

Influence of the CH_4/CO_2 ratio on reforming activity was further elucidated by varying the CO_2 quantity with a constant CH_4 and H_2O concentration in the inlet feed. Changes in the CO_2 concentration afforded negligible effects on CH_4 conversion at the temperatures employed (Fig. 12a). In contrast, CO_2 conversion decreased significantly as the CH_4/CO_2 ratio increased (Fig. 12b), which may result from the favored WGS reaction in the presence of low CO_2 concentration; i.e., low CO_2 concentration would drive the WGS reaction to increase the CO_2 conversion. H_2 yields obtained using the CH_4/CO_2 ratios were found to be comparable (Fig. 12c) while the H_2/CO ratio increased as the CH_4/CO_2 ratio increased (Fig. 12d). These results indicate that CO was converted into CO_2 via WGS for increased CH_4/CO_2 ratios (i.e., low CO_2 concentration). It is also worth noting that biogas (containing CH_4 and CO_2) reforming increased at higher temperatures leading to an increase in CH_4 consumption with increasing CO_2 concentration.

In Ni catalysts supported on reducible oxide supports including CeO_2 and Ce—ZrO_2, the oxygen vacancies of these supports have shown to initially activate CO_2 and the formed oxygen species were migrated into Ni-oxide interface, which further reacted with CH_x species produced by CH_4 dissociation on Ni [35,36]. Our Ni—Cr material, however, likely follows different reaction pathways to produce synthetic gas from the mixture of CH_4 and CO_2 since an irreducible oxide, Cr_2O_3 was involved. Note that the methane steam reforming process would be favored over methane dry reforming particularly in the presence of the S/C rations ranging from 1.5 to 3 (Fig. 11), implying that CO_2 activation at Cr_2O_3 surface is unlikely. Further study is needed to elucidate reaction pathways for the dry reforming.

4. Conclusions

The porous Ni—Cr plate manufactured by a conventional procedure exhibited very low catalytic activity. Pretreatment of the Ni—Cr plate catalyst by pre-oxidation at ≥600 °C and successive reduction at 700 °C enhanced the activity and stability of the plate catalyst. The surface of the bulk Ni—Cr material was reconstructed

during pretreatment to produce reactive Ni sites identified by SEM, TEM, and XPS-depth profiling studies. In the Ni—Cr catalyst, chromium oxide was proposed to play a crucial role in preventing agglomeration of the generated Ni active sites. The resulting activated Ni—Cr plate catalyst was highly active with enhanced stability for biogas reforming reactions at the steam/CH_4 ratio of $\geq$1.5 over a period of 100 h. Decreasing the CH_4/CO_2 ratios by increasing CO_2 concentrations afforded increased CO_2 conversions and decreased H_2/CO ratios, which were presumably due to the CO_2 reforming reaction and reverse water gas shift reaction. The developed pretreatment process could be employed to enhance the activity and durability of a Ni-based alloy catalyst for HTFCs equipped with an internal reforming system.

Acknowledgements

This research was supported by the Global Research Laboratory Program through the National Research Foundation of Korea funded by the Ministry of Science, ICT and Future Planning of Republic of Korea. Part of this research was also supported by the Fundamental Technology Development Programs for the Future through the Korea Institute of Science and Technology as well as by the National Research Foundation of Korea Grant funded by the Korean Government (MSIP) (University-Institute cooperation program.

Appendix A. Supplementary data

Supplementary data associated with this article can be found, in the online version, at http://dx.doi.org/10.1016/j.apcatb.2014.11.045.

References

[1] W.Z.J. Xu, Z. Li, J. Wang, J. Ma, Int. J. Hydrogen Energy 34 (2009) 6646–6654.
[2] W.Z.J. Xu, Z. Li, J. Ma, Int. J. Hydrogen Energy 35 (2010) 13013–13020.
[3] Y.H. Hu, E. Ruckenstein, Catal. Lett. 57 (1999) 167–169.
[4] A.S.K. Raju, C.S. Park, J.M. Norbeck, Fuel Process. Technol. 90 (2009) 330–336.
[5] A. Effendi, Z.G. Zhang, K. Hellgardt, K. Honda, T. Yoshida, Catal. Today 77 (2002) 181–189.
[6] P. Kolbitsch, C. Pfeifer, H. Hofbauer, Fuel 87 (2008) 701–706.
[7] A.L. Dicks, J. Power Sources 71 (1998) 111–122.
[8] S.P. Jiang, S.H. Chan, J. Mater. Chem. 39 (2004) 4405–4439.
[9] K.Y. Min, J.H. Kim, J.M. Bae, C.W. Yoon, S.W. Nam, J. Phys. Chem. C 116 (2012) 13281–13288.
[10] K.Y. Min, S.A. Hong, S.W. Nam, S.H. Seo, Y.S. Yoo, S.H. Lee, Int. J. Hydrogen Energy 36 (2011) 10247–10254.
[11] Z. Ma, R. Venkataraman, M. Farooque, J. Fuel Cell Sci. Technol. 7 (2010), 051003/1-051003/8.
[12] S.H. Kim, J.H. Chung, Y.T. Kim, J. Han, S.P. Yoon, S.W. Nam, T.H. Lim, H.I. Lee, Catal. Today 146 (2009) 96–102.
[13] Z.A. Sabirova, M.M. Danilova, V.I. Zaikovskii, N.A. Kuzin, V.A. Kirillov, T.A. Kriger, V.D. Meshcheryakov, N.A. Rudina, O.F. Brizitskii, L.N. Khrobostov, Kinet. Catal. 49 (2008) 428–434.
[14] S.H. Kim, S.W. Nam, T.H. Lim, H.I. Lee, Appl. Catal. B: Environ. 81 (2008) 97–104.
[15] Y. Ma, Y. Xu, M. Demura, D.H. Chun, G. Xie, T. Hirano, Catal. Lett. 112 (2006) 31–36.
[16] D.L. King, J.J. Strohm, X. Wang, H.S. Roh, C. Wang, Y.H. Chin, Y. Wang, Y. Lin, R. Rozmiarek, P. Singh, J. Catal. 258 (2008) 356–365.
[17] G. Bonura, C. Cannilla, F. Frusteri, Appl. Catal. B: Environ. 121–122 (2012) 135–147.
[18] D. Jung, I. Lee, H. Lim, D. Lee, J. Mater. Chem. 13 (2003) 1717–1722.
[19] M.W. Roberts, R.S.C. Smart, J. Chem. Soc, Faraday Trans. 1 (80) (1984) 2957–2968.
[20] A.P. Grosvenor, M.C. Biesinger, R.S.C. Smart, N.S. McIntyre, Surf. Sci. 600 (2006) 1771–1779.
[21] N.S. McIntyre, D.G. Zetaruk, D. Owen, Appl. Surf. Sci. 2 (1978) 55–73.
[22] L.M. Moroney, R.S.C. Smart, M.W. Roberts, J. Chem. Soc, Faraday Trans. 1 (79) (1983) 1769–1778.
[23] M. Witthaut, R. Cremer, K. Reichert, D. Neuschütz, Mikrochim. Acta 133 (2000) 191–196.
[24] G. Calvarin, R. Molins, A.M. Huntz, Oxid. Met. 53 (2000) 25–48.
[25] K.A. Hopskins, Oxidation of Metals and Alloys, Butteworth, London, 1967.
[26] N. Birks, G.H. Meier, F.S. Pettit, Introduction to High Temperature Oxidation of Metals, Cambridge University Press, New York, 2006.
[27] D.L. Douglass, Corros. Sci. 8 (1968) 665–678.
[28] M.F. Haroun, P.S. Moussounda, P. Légaré, Catal. Today 138 (2008) 77–83.
[29] J.C. Bertolini, Catal. Today 138 (2008) 84–96.
[30] C. Benndorf, C. Mundt, J Vac Sci Technol. A 10 (1992) 3026–3031.
[31] S.G. Wang, D.B. Cao, Y.W. Li, J. Wang, H. Jiao, Surf. Sci. 603 (2009) 2600–2606.
[32] H.S. Bengaard, J.K. Nørskov, J. Sehested, B.S. Clausen, L.P. Nielsen, A.M. Molenbroek, J.R. Rostrup-Nielsen, J. Catal. 209 (2002) 365–384.
[33] G. Ertl, H. Knözinger, F. Schüth, J. Weitkamp, Handbook of Heterogeneous Catalysis, 2008.
[34] S.Q. Chen, Y.D. Li, Y. Liu, X. Bai, Int. J. Hydrogen Energy 36 (2011) 5849–5856.
[35] D.K. Kim, K. Stöwe, F. Müller, W.F. Maier, J. Catal. 247 (2007) 101–111.
[36] F.B. Noronha, A. Shamsi, C. Taylor, E.C. Fendley, S.S. Williams, D.E. Resasco, Catal. Lett. 90 (2003) 13–21.